Diffracting Open-Ended Pipe Treated as a Lifting Surface

Rudolph Martinez*
Cambridge Acoustical Associates Inc., Cambridge, Massachusetts

The problem of diffraction by a rigid, open-ended pipe of negligible thickness and finite length is formulated and solved using the methodology of lifting-surface theory. The analysis assumes a still acoustic medium and considers incident fields corresponding to specified dipole sources. Among the possible applications is the preliminary but rigorous estimate of the shielding effect through pure diffraction of a cylindrical shroud on unsteady propeller forces prescribed within it . The present study confines itself to axisymmetric situations, including the simple case of a single harmonic force applied to the fluid along the cylinder's axis. The assumed zero thickness for the pipe wall results in a virtual source representation of unsteady doublets whose integrated component of radial velocity must cancel that of the incident field over the diffracting surface. For the single on-axis insonifying dipole the diffraction loading solution, or pressure difference between points just outside and inside the pipe, is checked by computing the resistive component of the acoustic admittance at the spatial origin of incident sound, and by verifying numerically that for each sample frequency this value of source input power matches the system's total radiated power.

Nomenclature

a	= cylinder radius (nondimensional)
a_m	= virtual load coefficient
F^h	= sectional blade load at hub
F^t	= sectional blade load at effective tip position
$J_\nu, H_\nu^{(1)}$	= Bessel, Hankel, and modified functions of order ν;
I_ν, K_ν	superscript (1) on H_ν is omitted throughout for simplicity of notation
k	= acoustic wavenumber (nondimensional)
$L/2$	= cylinder half length and normalizing constant
p^{inc}	= incident pressure field
$\Delta p(z)$	= diffraction loading, $p^o - p^i$, the difference between pressures on $r = a^+, a^-$ for $\lvert z\rvert < 1$
r	= radial coordinate (nondimensional)
r_h	= hub radius (nondimensional)
r_t	= effective tip radius (nondimensional)
R	$= \sqrt{r^2 + (z-\hat{z})^2}$
U_n	= nth Chebyshev polynomial of 2nd kind
z	= axial coordinate with origin at cylinder midaxis (nondimensional)
$\hat{z}$	= axial position of sources as measured from midaxis point $z = 0$ (nondimensional)
γ	$= \sqrt{k^2 - \bar{k}^2}$, $\bar{k}$ is running wavenumber
ρc	= characteristic fluid impedance
θ	$= \tan^{-1} r/z$
$\hat{\theta}$	$= \tan^{-1}[r/(z-\hat{z})]$

Introduction

THE classical solution for diffraction of sound sources in an unflanged pipe is by Levine and Schwinger,[1] who considered a semi-infinite geometry and a plane-wave incident field. Their development hinged on an analytical step, then somewhat controversial,[2] via which the Helmholtz integral was differentiated with respect to the normal radial coordinate prior to the main attack in wave number space using the Wiener-Hopf technique. Had the problem been kept instead in spatial coordinates, the derived expression would have displayed explicitly the second-order Mangler singularity familiar to workers in wing theory.[3] The present study takes up this unpursued spatial formulation in the solution of the field radiating from a rigid pipe equally thin but of finite length.

Since Ref. 1 (1948), many modern analyses of acoustic scattering by closed bodies in unbounded media have been based on discretizations of the Helmholtz integral, e.g., Schuster and Smith,[4] and on patch-up techniques applied at or near frequencies where the formulation fails mathematically: at the resonances of the artificial cavity carved out of the fluid by the scattering body. Schenck[5] fulfills the latter task through a coupling of actual exterior and "interior" Helmholtz problems. The method of Burton and Miller[6] (cf. also Mathews and Hitchings[7]), however, circumvents it completely with the combination of the Helmholtz integral and its above-cited differentiated version to yield a system regular for all frequencies. It is, therefore, somewhat surprising, given the established success of thin-wing theory, to find that at least some numerical implementations of this second approach apparently break down for lamina-like diffracting shapes.[8] The present computation of diffraction loads across the thin wall of a cylindrical noise shroud demonstrates that the differentiated, or "lifting-surface," form is not only well posed for such geometries, but is also the only one necessary. We express the solution in terms of Chebyshev polynomials and thereby are able to evaluate the kernel's steady and singular contribution in closed form—a procedure that should be equally useful in treating the spanwise load behavior for a wing in subsonic flow [rather than the expansion in Eq. (13) of Ref. 3, for example]. We should point out that Hamdi and Ville[9] have already precisely solved our pipe diffraction problem using a variational technique especially tailored to scattering. At the outset this technique eliminates the kernel's singularity, but it does not seem to be immediately applicable to the spanwise part of the lifting-surface equation.

Two insonifying source configurations will be considered, both axisymmetric: 1) a single harmonic force $F_o e^{-i\omega t}$ driving the fluid along the axis at position $\hat{z}$ (Fig. 1), and 2) the angular average of a radial spread of similar forces modeling blade thrusts on a propeller, or turbofan. The inclusion of a duct lining and of more complicated incident sources are deferred to a forthcoming paper (lack of circumferential symmetry for incident sources simply resulting in a Fourier series in ϕ, the separable circumferential coordinate, and in a set of uncoupled modal integral equations). We confine our

Presented as Paper 86-1952 at the AIAA 10th Aeroacoustics Conference, Seattle, WA, July 9-11, 1986; received July 29, 1986; revision received July 2, 1987.

*Senior Scientist. Member AIAA.

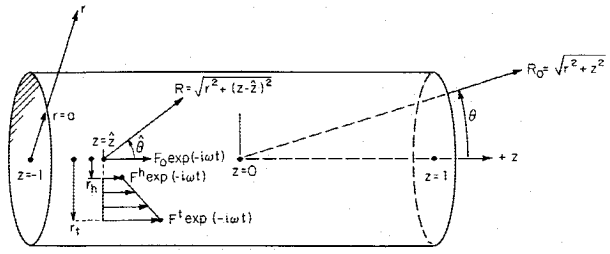

Fig. 1 Model geometry showing (r,z,θ) coordinate systems and incident field configurations.

analysis to axisymmetric cases, paying special attention to the single force, because an important power check is then readily carried out on both formulation and numerical treatment of the problem. Thus, the balance between the computed resistive component of acoustic admittance at the axial station of incident sound, and the acoustic energy radiated by combined incident and scattered fields, will prove that the pipe itself generates no power and that flow tangency has been satisfied over the solid boundary.

A vast body of literature exists on the acoustic characteristics of ducts with or without mean flow, as in respective recent examples: Horowitz et al.[10] and Nayfeh et al.,[11] and Fuller[12] and Prasad.[13] The significant physical mechanisms of noise production are essentially different for the two groups. In the former case, much attention has been devoted to the effects of the incident field on the stability of exhaust flow (from a trailing-edge pipe), and to such issues as whether a full Kutta condition should be enforced at the exit station given typical thicknesses of shear layers there (Orszag and Crow,[14] and Crighton[15,16]). These decisions are important because they bear sensitively on the character and magnitude of the acoustic prediction. For example, using a thin-shear layer model (full Kutta condition), Munt[17] has found that, in contrast to several previous investigations, jet noise due to the instability mechanism should dominate within a 45 deg sector about the wake, and that this type of radiation weakens when an exterior flow is imposed, i.e., when the speed of the jet diminishes relative to that of flight.

In placing the pipe in question in a stationary "free-flooding" medium, the present study focuses on the purely diffractive effect. The study belongs in the category of Refs. 12, 13 but without relying on either semi-empirical results[13] or on a spatial match to the exterior medium.[12] Consistently, the proposed interpretation of the incident field in terms of unsteady blade loads implies a model that isolates this direct noise blockage mechanism for the shroud while ignoring all viscous and potential freestream effects.

Formulation

The idealized cylindrical surface will be taken to be of zero thickness and perfectly rigid, with the normal component of velocity continuous across it for both fields, incident and scattered. This follows because the as yet undetermined source distribution must be such that it "cancels" the normal component of incident particle velocity at every point of the rigid interior and exterior cylindrical surfaces. Since by virtue of the object's infinitesimal thickness the value of the incident normal particle velocity does not change across it, the cancelling component, i.e., the scattered field's normal velocity, must be for $r=a^-$ the same as for $r=a^+$. Moreover, since along the two $|z|>1$, $r=a$ artificial baffling surfaces all physical variables are continuous, the normal component of scattered particle velocity is continuous across $r=a$ for all z.

Letting $p^{o,i}$ stand respectively for the assumed form of solutions of the scattered pressure for $r>a$, $r<a$, one obtains

$$p^o(r,z)=\int_{-\infty}^{\infty} d\bar{k}e^{-i\bar{k}z}\frac{J_o'(\gamma a)}{H_o'(\gamma a)}H_o(\gamma r)A(\bar{k}) \tag{1}$$

$$p^i(r,z)=\int_{-\infty}^{\infty} d\bar{k}e^{-i\bar{k}z}J_o(\gamma r)A(\bar{k}) \tag{2}$$

so that $\partial p^o(r=a,|z|<\infty)/\partial r=\partial p^i(r=a,|z|<\infty)/\partial r$. In the above

$$\gamma=\sqrt{k^2-\bar{k}^2}\ (=i\sqrt{\bar{k}^2-k^2}\ \text{for}\ |\bar{k}|>k)$$

where k is the nondimensional acoustic wave number $\omega L/2c$.

Subtracting Eq. (2) from Eq. (1) yields for $r=a$ and all z

$$p^o-p^i=\int_{-\infty}^{\infty} d\bar{k}e^{-i\bar{k}z}A(\bar{k})\left\{\frac{J_o'(\gamma a)}{H_o'(\gamma a)}H_o(\gamma a)-J_o(\gamma a)\right\} \tag{3}$$

where the term in brackets may be simplified to

$$-\frac{2i}{\pi\gamma a}\frac{1}{H_o'(\gamma a)}=\frac{2i}{\pi\gamma a H_1(\gamma a)} \tag{4}$$

by means of the Bessel functions' Wronskian relationship. Inverting Eq. (3) and enforcing continuity of pressure on $r=a$ for $|z|>1$ yields

$$A(\bar{k})=-\frac{i\pi}{2}\gamma a H_1(\gamma a)\int_{-1}^{1}\frac{dz}{2\pi}e^{i\bar{k}z}[p^o-p^i] \tag{5}$$

Calling $p^o(a,z)-p^i(a,z)=\Delta p(z)$ for compactness, we thus have

$$p^o(r,z)=-\int_{-1}^{1}\frac{d\bar{z}}{2\pi}\Delta p(\bar{z}) \times\int_{-\infty}^{\infty}d\bar{k}e^{-i\bar{k}(z-\bar{z})}\frac{i\pi}{2}\gamma a J_1(\gamma a)H_o(\gamma r) \tag{6}$$

and

$$p^i(r,z)=-\int_{-1}^{1}\frac{d\bar{z}}{2\pi}\Delta p(\bar{z}) \times\int_{-\infty}^{\infty}d\bar{k}e^{-i\bar{k}(z-\bar{z})}\frac{i\pi}{2}\gamma a H_1(\gamma a)J_o(\gamma r) \tag{7}$$

The validity of the interchange of orders integration from Eq. (5) to either Eqs. (6) or (7) is guaranteed by the uniform convergence of the $\bar{k}$ integral for $r\neq a$.

Now, for $|\bar{k}|>k$, the following relations hold [Ref. 18, p. 375, Eqs. 9.6.3(a), 9.6.4(a)]:

$$\frac{i\pi}{2}\gamma a J_1(\gamma a)H_o(\gamma r)=-\sqrt{-\gamma^2}aI_1(\sqrt{-\gamma^2}a)K_o(\sqrt{-\gamma^2}r) \tag{8a}$$

$$\frac{i\pi}{2}\gamma a H_1(\gamma a)J_o(\gamma r)=\sqrt{-\gamma^2}aK_1(\sqrt{-\gamma^2}a)I_o(\sqrt{-\gamma^2}r) \tag{8b}$$

The derivation of the integral equation for the cylinder as a lifting surface may be carried out using either equation pairs (6) and (8a), or (7) and (8b). We proceed here with the former. For $|\bar{k}|\gg k$ (Ref. 18, p. 377, Eq. 9.7.1 and p. 378,

Eq. 9.7.2) Eq. (8a) yields

$$-\sqrt{-\gamma^2}aI_1(\sqrt{-\gamma^2}a)K_o(\sqrt{-\gamma^2}r)$$
$$\sim -\frac{e^{-\sqrt{-\gamma^2}(r-a)}}{2}\{1+0(-\gamma^2)^{-1/2}\} \tag{9}$$

so that, adding and subtracting, one may write

$$p^o(r,z) = -\int_{-1}^{1}\frac{d\bar{z}}{2\pi}\Delta p(\bar{z})$$
$$\times\int_{-\infty}^{\infty} d\bar{k}e^{-i\bar{k}(z-\bar{z})}\left\{\frac{i\pi}{2}\gamma a J_1(\gamma a)H_o(\gamma r)+\frac{e^{-\sqrt{-\gamma^2}(r-a)}}{2}\right\}$$
$$+\int_{-1}^{1}\frac{d\bar{z}}{2\pi}\Delta p(\bar{z})\int_{-\infty}^{\infty}\frac{d\bar{k}}{2}e^{-i\bar{k}(z-\bar{z})-\sqrt{-\gamma^2}(r-a)} \tag{10}$$

Differentiating with respect to r, carrying out a careful limiting process detailed in Ref. 19, and setting the left side of the equation equal to

$$-\frac{\partial p^{\text{inc}}}{\partial r}$$

on $r=a$, $|z|<1$ yields the governing integral equation:

$$-\frac{\partial p^{\text{inc}}}{\partial r}(a,|z|<1)=\int_{-1}^{1}d\bar{z}\Delta p(\bar{z})K_{\text{reg}}(z-\bar{z})$$
$$+\frac{1}{2\pi}\text{⨍}_{-1}^{1}\frac{d\bar{z}\Delta p(\bar{z})}{(z-\bar{z})^2} \tag{11}$$

where $K_{\text{reg}}(z-\bar{z})$ stands for the regular part of the kernel:

$$K_{\text{reg}}(z-\bar{z})=\frac{ik^2}{4}\left(1+\frac{3}{8k^2a^2}\right)H_o(k|z-\bar{z}|)$$
$$+\frac{ik^2}{4}\left[H_2(k|z-\bar{z}|)-\frac{H_1(k|z-\bar{z}|)}{k|z-\bar{z}|}\right]-\frac{1}{2\pi(z-\bar{z})^2}$$
$$+\int_{-\infty}^{\infty}d\bar{k}e^{-i\bar{k}(z-\bar{z})}\left\{\frac{i}{4}\gamma^2 aH_1(\gamma a)J_1(\gamma a)\right.$$
$$\left.+\frac{\sqrt{-\gamma^2}}{4\pi}-\frac{3}{32\pi a^2}\frac{1}{\sqrt{-\gamma^2}}\right\} \tag{12}$$

On the second term on the right side of Eq. (11) we have applied the (×) symbol for a second-order improper integral, the standard nomenclature used in wing theory, e.g., Watkins et al.:[3]

$$\text{⨍}_{-1}^{1}\frac{d\bar{z}\Delta p(\bar{z})}{(z-\bar{z})^2}\equiv\lim_{\epsilon\to 0}\left\{\left(\int_{-1}^{z-\epsilon}+\int_{z+\epsilon}^{1}\right)\frac{d\bar{z}\Delta p(\bar{z})}{(z-\bar{z})^2}-\frac{2\Delta p(z)}{\epsilon}\right\} \tag{13}$$

Calculation of the Acoustic Field

The radiated far field follows from the $\Delta p(z)$ solution. One begins with Eq. (6) and the large-r asymptotic of $H_o(\gamma r)$:

$$\lim_{\sqrt{r^2+z^2}\to\infty} p^o(r,z) = -\frac{e^{i\pi/4}}{2^{3/2}}\frac{1}{\sqrt{\pi}}\frac{a}{\sqrt{r}}$$
$$\times\int_{-1}^{1}d\bar{z}\Delta p(\bar{z})\int_{-\infty}^{\infty}d\bar{k}\sqrt{\gamma}J_1(\gamma a)e^{-i\bar{k}(z-\bar{z})+i\gamma r} \tag{14}$$

Now, from the saddle point at $\bar{k}=-k\cos\theta$ we obtain[20]

$$\lim_{\sqrt{r^2+z^2}\to\infty}\int_{-\infty}^{\infty}d\bar{k}\sqrt{\gamma}J_1(\gamma a)e^{-i\bar{k}(z-\bar{z})+i\gamma r}$$
$$\sim\frac{\sqrt{2\pi}k}{(r^2+z^2)^{1/4}}e^{-i\pi/4}(\sin\theta)^{3/2}J_1(ka\sin\theta)$$
$$\times\exp\{i(k\sqrt{r^2+z^2}-k\bar{z}\cos\theta)\} \tag{15}$$

where $r/\sqrt{r^2+z^2}=\sin\theta$. Substituting Eq. (15) into Eq. (14) yields

$$\lim_{\sqrt{r^2+z^2}\to\infty}p^o\sim-\frac{ka(\sin\theta)^{3/2}}{2\sqrt{r}(r^2+z^2)^{1/4}}e^{ik\sqrt{r^2+z^2}}$$
$$\times J_1(ka\sin\theta)\int_{-1}^{1}d\bar{z}\Delta p(\bar{z})e^{-ik\bar{z}\cos\theta} \tag{16}$$

Finally, since $\sqrt{r}(r^2+z^2)^{1/4}=\sqrt{r^2+z^2}\sqrt{\sin\theta}$, we have

$$p^o(\sqrt{r^2+z^2},\theta)\sim-\frac{ka}{2}\frac{e^{ik\sqrt{r^2+z^2}}}{\sqrt{r^2+z^2}}$$
$$\sqrt{r^2+z^2}\to\infty$$
$$\times\sin\theta J_1(ka\sin\theta)\int_{-1}^{1}d\bar{z}\Delta p(\bar{z})e^{-ik\bar{z}\cos\theta} \tag{17}$$

Strictly speaking, the above does not hold at the $\theta=0,\pi$ far-field points on the cylinder axis because it was derived from the p^o solution. However, continuity of pressure anywhere but on the cylinder surface allows the result to be physically continued to include these two points. That the scattered field vanishes at $\theta=0,\pi$ is consistent with our classification of the problem as a purely lifting one, i.e., one with continuous normal velocities across a scattering surface that is essentially colinear with the two far-field points in question.

The total far-field pressure p is given by the sum of the incident field and the above scattered component:

$$\lim_{\sqrt{r^2+z^2}\to\infty}p(\sqrt{r^2+z^2},\theta)=\lim_{\sqrt{r^2+z^2}\to\infty}p^{\text{inc}}+\text{Eq. (17)} \tag{18}$$

Solution by Chebyshev Polynomial Expansion

The acoustic load (due to the scattered component) on the cylindrical surface should vanish as $\sqrt{1-z}$ as $z\to 1^-$, and as $\sqrt{z+1}$ as $z\to -1^+$ (e.g., Noble,[20] p. 74). A natural form for the solution is in terms of Chebyshev polynomials of the second kind $U_n(z)$ defined as (Ref. 18, p. 776, Eqs. 22.3.16):

$$U_n(\cos\psi)=\frac{\sin(n+1)\psi}{\sin\psi} \tag{19}$$

We let

$$\Delta p(\bar{z})=\sqrt{1-\bar{z}^2}\sum_{n=0}^{N}a_nU_n(\bar{z}) \tag{20}$$

where N is an integer of sufficient size. Since the $U_n(z=\pm 1)$ are never zero the above solution is guaranteed to have the correct algebraic behavior as $z\to\pm 1$. But also, we note by

differentiation of Eq. 22.13.4, Ref. 18, p. 785, that[19]

$$\oint_{-1}^{1} \frac{d\bar{z}\sqrt{1-\bar{z}^2}}{(z-\bar{z})^2} U_n(\bar{z}) = -\pi(n+1)U_n(z) \tag{21}$$

Substituting Eq. (20) into Eq. (11) and using Eq. (21) yields

$$-\frac{\partial p^{\text{inc}}}{\partial r}(a, |z|<1) = -\frac{1}{2}\sum_{n=0}^{N} a_n(n+1)U_n(z) + \sum_{n=0}^{N} a_n \int_{-1}^{1} d\bar{z} K_{\text{reg}}(z-\bar{z}) U_n(\bar{z})\sqrt{1-\bar{z}^2} \tag{22}$$

Finally, we multiply through by $\sqrt{1-z^2}U_m(z)$, integrate with respect to z from -1 to $+1$, and invoke the orthogonality relation

$$\int_{-1}^{1} dz\sqrt{1-z^2}U_m(z)U_n(z) = \begin{cases} 0 & \text{if } m \neq n \\ \pi/2 & \text{if } m = n \end{cases} \tag{23}$$

to yield a linear system for the a_n coefficients

$$\sum_{n=0}^{N} B_{mn}a_n = F_m, \qquad m = 0,1,\ldots,N \tag{24}$$

where

$$B_{mn} = B_{nm} = -\frac{\pi}{4}(m+1)\delta_{mn} + \int_{-1}^{1} dz\sqrt{1-z^2}U_m(z) \times \int_{-1}^{1} d\bar{z}\sqrt{1-\bar{z}^2}U_n(\bar{z})K_{\text{reg}}(z-\bar{z}) \tag{25}$$

$$F_m = -\int_{-1}^{1} dz\sqrt{1-z^2}U_m(z)\frac{\partial p^{\text{inc}}}{\partial r}(a, |z|<1) \tag{26}$$

where δ_{mn} is the Kronecker delta function. After some algebra the B_{mn} elements are found to be given by[19]

$$\begin{aligned} B_{mn} = B_{nm} = &-\frac{\pi}{4}(m+1)\delta_{mn} \\ &+ \pi^2(m+1)(n+1)\cos\left[(m-n)\frac{\pi}{2}\right] \\ &\times \left\{\int_0^{\pi/2} d\xi \sin\xi \frac{J_{m+1}(k\cos\xi)J_{n+1}(k\cos\xi)}{\cos^2\xi} \right. \\ &\times \left[\frac{ika}{2}\sin^2\xi H_1(ka\sin\xi)J_1(ka\sin\xi) + \frac{\cos\xi}{2\pi}\right] \\ &+ \int_0^{\infty} d\xi \sinh\xi \frac{J_{m+1}(k\cosh\xi)J_{n+1}(k\cosh\xi)}{\cosh^2\xi} \\ &\times \left[-\frac{ka}{\pi}\sinh^2\xi K_1(ka\sinh\xi)\right. \\ &\left.\left.\times I_1(ka\sinh\xi) + \frac{\cosh\xi}{2\pi}\right]\right\} \end{aligned} \tag{27}$$

so that $B_{mn} = 0$ if $m+n$ is odd. In the above we have used the identity

$$\int_{-1}^{1} dz\sqrt{1-z^2}U_m(z)e^{-ikz} = \pi(m+1)e^{-im\pi/2}\frac{J_{m+1}(\bar{k})}{\bar{k}} \tag{28}$$

When the incident field is due to a point force in the axial direction $F_o e^{-i\omega t}$, applied directly to the fluid at normalized axial position $\hat{z}$, Eq. (26) becomes

$$F_m = \frac{F_o}{L^2}\cdot\frac{a}{\pi}\int_0^{\pi} d\psi \sin\psi \sin[(m+1)\psi](\cos\psi - \hat{z})e^{ikR} \times \left\{-\frac{k^2}{R^3} - \frac{3ik}{R^4} + \frac{3}{R^5}\right\} \tag{29}$$

where $R = \sqrt{a^2 + (\cos\psi - \hat{z})^2}$

Power Balance for Incident Field Due to a Single Dipole

The question must now be asked whether the numerically calculated solution of Eq. (24), with B_{mn} defined by Eq. (27), truly satisfies the condition of zero total velocity on the diffracting cylinder. Since our lifting surface integral equation is first and foremost a direct statement of flow tangency at the scattering surface, it would initially seem that little can be done towards checking the solution beyond simply making sure that matrix B_{mn} has been inverted correctly. However, such a calculation would say nothing about the validity of the analytical/numerical generation of the kernel. The primary purpose of the calculation of radiated and source-input powers that follow will be to provide this needed check.

Let us assume for the moment that the pressure solution corresponding to system Eq. (24) is inconsistent with the zero flow-through condition that we think has been satisfied, i.e., that the "solution" corresponds, instead, to a partially permeable or compliant boundary. But such a boundary would generally either dissipate or generate energy, unless, through some analytical/numerical coincidence, it behaved reactively for all frequencies—an extremely unlikely event given the complicated pattern of complex entries in B_{mn}. We shall compute the total power radiated to the far field by our solution and, in a separate independent calculation, the energy that the dipole source injects into the medium in the presence of the diffracting object. The balance of these two will prove that the cylindrical boundary is always reactive, or by the above argument, always infinite in impedance for all frequencies calculated. The numerical demonstration of this balance presented below, therefore, constitutes a check not only on predicted far-field pressure levels, but also on the entire formulation and analysis of the problem.

Radiated Power

The incident field p^{inc} due to a force $F_o e^{-i\omega t}$ applied directly to the fluid at axial position $\hat{z}$ in the direction of the cylinder axis (Fig. 1)[21] is

$$\left(\frac{L}{2}\right)^2 \cdot p^{\text{inc}} = -\frac{F_o}{4\pi}\frac{\partial}{\partial z}\frac{e^{ikR}}{R} = -\frac{F_o}{4\pi R^2}(ikR-1)e^{ikR}\cos\hat{\theta} \tag{30}$$

where

$$R = \sqrt{r^2 + (z-\bar{z})^2} \tag{31a}$$

$$\hat{\theta} = \tan^{-1}\left[\frac{r}{z-\hat{z}}\right] \tag{31b}$$

R and $\hat{\theta}$ are, respectively, normalized range and directivity angle measured from a source-based coordinate system. The magnitude of the total radiated pressure normalized by the

on-axis incident field pressure is given by Eqs. (18), (30), to be

$$\lim_{R_o-\infty}\frac{|p|}{|p^{\text{inc}}(\theta=0)|}=\left|i\cos\theta e^{-ik\hat{z}\cos\theta}+\left(\frac{L^2a}{2F_o}\right)\pi^2\sin\theta J_1(ka\sin\theta)\times\sum_{m=0}^{N}a_m(m+1)e^{\mp im\pi/2}\frac{J_{m+1}(|k\cos\theta|)}{|k\cos\theta|}\right| \tag{32}$$

The $\mp$ signs in $\exp(\mp im\pi/2)$ correspond to $0<\theta<\pi/2$, $\pi/2<\theta<\pi$, respectively. We recall that the a_m's have dimension of pressure that cancels that of the group L^2/F_o. The phase factor $\exp(-ik\hat{z}\cos\theta)$ is the result of Taylor-expanding R about R_o in Eq. (30), i.e, $kR\simeq kR_o-k\hat{z}\cos\theta$, where

$$R_o=\sqrt{r^2+z^2}$$

The period-averaged power radiated by the free-dipole/diffracting-cylinder system is given by

$$\Pi_{\text{rad}}=\frac{1}{2\rho c}\int\int_S dS\,|p|^2 \tag{33}$$

where $dS=(L/2)^2 2\pi R_o^2\sin\theta\,d\theta$, due to the axisymmetry; ρc is the fluid's characteristic impedance. Thus we have

$$\frac{\Pi_{\text{rad}}}{\Pi_{\text{rad}}^{\text{inc}}}=\frac{3}{2}\int_0^\pi d\theta\sin\theta\times\left|i\cos\theta e^{-ik\hat{z}\cos\theta}+\frac{L^2a}{2F_o}\pi^2\sin\theta J_1(ka\sin\theta)\times\sum_{m=0}^{\infty}a_m(m+1)e^{\mp im\pi/2}\frac{J_{m+1}(|k\cos\theta|)}{|k\cos\theta|}\right|^2 \tag{34}$$

where the power radiated by the dipole's incident field alone [Eqs. (39), (33)] is

$$\left(\frac{L}{2}\right)^2\cdot\Pi_{\text{rad}}^{\text{inc}}=\frac{F_o^2k^2}{16\pi\rho c}\int_0^\pi d\theta\sin\theta\cos^2\theta=\frac{F_o^2k^2}{24\pi\rho c} \tag{35}$$

in agreement with Lamb.[22]

Source Input Power

To calculate the input power directly it is convenient to isolate a small fluid sphere of radius R around the dipole source. The sphere must be small enough that the fluid within it moves as a rigid body under the pulling action of the applied force. We apply the standard nomenclature that more generally describes the radial velocity $\dot{w}$ of the sphere's surface in terms of modal functions f_ng_m (polar trigonometic functions and spherical harmonics)

$$\dot{w}=\sum_{n,m}\dot{w}_{mn}f_ng_m$$

Under the restrictions cited, the above collapses to simply $\dot{w}_{01}\cos\hat{\theta}$, where the "0" subscript reflects the axisymmetry by considering only the zeroth circumferential mode, and the second "1" subscript corresponds to the rigid-body, axial-direction mode coefficient of $\cos\hat{\theta}$. Besides the applied drive F_o, a system of surface pressure loads the sphere throughout its motion. There are two contributions: 1) hydrodynamic loading that the sphere would feel were the fluid unbounded, and 2) extra loading due solely to the presence of the cylinder, which may be taken to act as a partial reflector of the flow under the former contribution. These two contributions are obtained from the pressures provided by Eqs. (30) and (7), respectively.

The governing equation (Newton's 2nd law) for the sphere's motion is

$$\left(\frac{L}{2}\right)^3\left(-i\omega\frac{4\pi R^3}{3}\right)\rho\dot{w}_{01}=F_o-\left(\frac{L}{2}\right)^2\int_0^\pi[p(R,\hat{\theta})\cdot\cos\hat{\theta}](2\pi R^2\sin\hat{\theta}\,d\hat{\theta}) \tag{36}$$

In the above, $p(R,\hat{\theta})$, at any instant, acts in the radial direction by definition of pressure, or normal stress, in an inviscid flow. The multiplying $\cos\hat{\theta}$ factor accounts for the component of loading in the direction of motion.

Just as $\dot{w}$, p must be given by just $p_{01}\cos\hat{\theta}$, and Eq. (36) becomes

$$\left(\frac{L}{2}\right)^3\left(\frac{-i\omega 4\pi R^3}{3}\right)\rho\dot{w}_{01}=F_o-\left(\frac{L}{2}\right)^2\frac{4\pi R^2}{3}p_{01} \tag{37}$$

The input power is given by

$$\Pi_{\text{input}}=\frac{1}{2}Re[F_o\dot{w}_{01}^*]=\frac{F_o}{2\rho c\cdot kR}Im\{p_{01}\} \tag{38}$$

where the first term on the right side of Eq. (37) does not contribute because the drive F_o is in phase with itself. Here "*" denotes complex conjugate.

A ready check on Eq. (38) is obtained by applying it to the case of the free dipole. Then, from Eq. (30)

$$\left(\frac{L}{2}\right)^2\cdot p_{01}^{\text{inc}}=-\frac{F_o}{4\pi R^2}(ikR-1)e^{ikR}=\frac{iF_o}{12\pi R^2}(kR)^3 \tag{39}$$

as far as the imaginary part is concerned. Introducing the last result of Eq. (39) into Eq. (38) yields

$$\left(\frac{L}{2}\right)^2\cdot\Pi_{\text{input}}^{\text{inc}}=\frac{F_o^2k^2}{24\pi\rho c} \tag{40}$$

which reproduces the result of Eq. (35) and thereby confirms the principle of energy conservation without the cylinder.

Including the presence of the cylinder, our goal is to derive an analytic expression for the total input power based on

$$p_{01}^{\text{inc}}+p_{01}^{i}$$

and, thus, to check the numerical results of Eq. (34) using near-field quantities. The solution will use the p^i part of the scattered pressure solution rather than the p^o part used in the analysis so far:

$$\Pi_{\text{input}}=\frac{F_o}{2\rho ckR}Im\{p_{01}^{\text{inc}}+p_{01}^{i}\}=\left(\frac{2}{L}\right)^2\cdot\frac{F_o^2k^2}{24\pi\rho c}+\frac{F_o}{2\rho ckR}Im\{p_{01}^{i}\} \tag{41}$$

By definition p_{01}^i is obtained from

$$p_{01}^{i}(R)=\frac{1}{\pi}\int_0^{2\pi}d\hat{\theta}\cos\hat{\theta}p^i(R,\hat{\theta}) \tag{42}$$

or

$$p'_{01} = -\frac{1}{\pi}\int_{-1}^{1}\frac{d\bar{z}}{2\pi}\Delta p(\bar{z})\int_{-\infty}^{\infty} dk e^{-ik(\hat{z}-\bar{z})}\frac{i\pi\gamma a}{2}H_1(\gamma a)$$
$$\times\int_0^{2\pi} d\hat{\theta}\cos\hat{\theta}J_o(\gamma R\sin\hat{\theta})e^{-ikR\cos\hat{\theta}} \quad (43)$$

by virtue of Eq. (7). The propriety of the interchange of integration orders is again guaranteed by the uniform convergence of the $\bar{k}$ integral whenever $r\neq a$. We have used $z=\hat{z}+R\cos\hat{\theta}$, $r=R\sin\hat{\theta}$ as required by the local coordinate system on the elemental sphere.

The $\hat{\theta}$ integral may be calculated to be[19] $\{k\cong\bar{k}\}$

$$\int_0^{2\pi} d\hat{\theta}\cos\hat{\theta}e^{-ikR\cos\hat{\theta}}\begin{Bmatrix} J_o(\gamma R\sin\hat{\theta}) \\ I_o(\sqrt{-\gamma^2}R\sin\hat{\theta}\end{Bmatrix}$$
$$= -\pi i\{J_o[\,|k-\bar{k}|R/2]J_1[\,|k+\bar{k}|R/2]\,|1+\bar{k}/k|$$
$$-J_o[\,|k+\bar{k}|R/2]J_1[\,|k-\bar{k}|R/2]\,|1-\bar{k}/k|\} \quad (44)$$

where the absolute-value signs are introduced for convenience of using positive arguments in the computation of the Bessel functions. Finally, substituting Eq. (44) into Eq. (43) and using Eq. (41) gives

$$\Pi_{\text{input}} = \left(\frac{2}{L}\right)^2\cdot\frac{F_o^2k^2}{24\pi\rho c}+\frac{F_o\pi aL}{8\rho ck}Re\Big[\sum_{m=0}^{N}a_m(m+1)$$
$$\times\int_0^{\infty} d\bar{k}\gamma H_1(\gamma a)\frac{J_{m+1}(\bar{k})}{\bar{k}}\sin\left(\bar{k}\hat{z}-\frac{m\pi}{2}\right)$$
$$\times\frac{1}{R}\{J_o[\,|k-\bar{k}|R/2]J_1[\,(k+\bar{k})R/2](1+\bar{k}/k)$$
$$-J_o[\,(k+\bar{k})R/2]J_1[\,|k-\bar{k}|R/2]\,|1-\bar{k}/k|\}\Big] \quad (45)$$

where the $1/R$ term in the coefficient factor has been grouped with the Bessel function product term. Just as intermediate manipulations buried in Eq. (39) were not really necessary because numerical results of Eq. (38) with

$$p_{01}=p_{01}^{\text{inc}}$$

as given by the first equality of Eq. (39) would yield the correct result, we may keep the "exact" form of Eq. (45), which is for a sphere of finite radius R, or we may approximate it analytically for $R\to 0$ in a manner analogous to the last step of Eq. (39). The approximation approach is tentatively justified by the rapid exponential decay of the $\bar{k}$ integral since

$$H_1(\gamma a)\sim e^{-a\sqrt{-\gamma^2}}$$

for $\bar{k}\gg k$, so that the largest contribution to the integral in Eq. (45) comes from the neighborhood of the lower limit. We let R go to zero:

$$\lim_{R\to 0}\frac{1}{R}\{J_o[\,|k-\bar{k}|R/2]J_1[\,(k+\bar{k})R/2]\,(1+\bar{k}/k)$$
$$-J_o[\,(k+\bar{k})R/2]J_1[\,|k-\bar{k}|R/2]\,|1-\bar{k}/k|\}=\bar{k} \quad (46)$$

so that

$$\Pi_{\text{input}} = \left(\frac{2}{L}\right)^2\cdot\frac{F_o^2k^2}{24\pi\rho c}+\frac{F_o\pi ka}{4\rho c}$$
$$\times\text{Re}\Big\{\sum_{m=0}^{N}a_m(m+1)\Big[\int_0^{\pi/2} d\xi\,\sin^2\xi H_1(ka\sin\xi)$$
$$\times J_{m+1}(k\cos\xi)\sin\left(k\hat{z}\cos\xi-\frac{m\pi}{2}\right)$$
$$-\frac{2i}{\pi}\int_0^{\infty} d\xi\,\sinh^2\xi K_1(ka\sinh\xi)J_{m+1}(k\cosh\xi)$$
$$\times\sin\left(k\hat{z}\cosh\xi-\frac{m\pi}{2}\right)\Big]\Big\} \quad (47)$$

where $-2i/\pi$ times the second integral contributes because the a_m Chebyshev polynomial coefficients (that have dimensions of pressure) are generally complex. It should be noted that since a_m is proportional to F_o, both terms in the above are proportional to F_o^2.

Solution for a Radial Distribution of Blade Forces

The solution of the problem using the single dipole for incident field will provide a check on the analytical treatment of the integral equation's kernel and on the numerical schemes used to generate the related B_{mn} matrix. With the confidence thus gained, we now change the incident field to that corresponding to a distribution of dipoles that more realistically models a system of unsteady blade forces. Obviously, the generalization does not affect the equation's kernel, all changes being confined to the F_m right side of Eq. (24).

The new distribution will still be oriented in the axial direction and will model only the effect of time-varying blade thrusts. Also, in keeping with the axisymmetric formulation of the scattering problem, only the zeroth circumferential mode (i.e., angular average) of such blade loading is used. We neglect differences in the axial position of blade points due to blade twist and so take the distribution to be coplanar, extending at axial station $\hat{z}$ over the area defined by concentric circles of radii r_h and r_t (Fig. 1); r_h denotes true hub radius while r_t stands for effective tip radius, taken here as the radial section where propeller blades typically measure maximum sectional loads, e.g., the 60–70% outboard point. In cutting off the loading at r_t, we neglect only its rapidly decaying part between this position and actual blade tip, with the modeling advantage that the radial distribution can then assume a simple monotonically increasing functional form between r_h and r_t.

The assumed time dependence of blade loads will be nontonal and with a broadband frequency spectrum as coefficient of $e^{-i\omega t}$.

Analysis for Axisymmetric Distribution

We generalize Eq. (30) as follows:

$$\left(\frac{L}{2}\right)\cdot p^{\text{inc}}(r,\phi) = -\frac{1}{4\pi}\frac{\partial}{\partial z}\int_{r_h}^{r_t} dr_o\int_0^{2\pi} d\phi_o$$
$$F(r_o,\phi_o)\frac{e^{ik\sqrt{r^2+r_o^2-2rr_o\cos(\phi-\phi_o)+(z-\hat{z})^2}}}{\sqrt{r^2+r_o^2-2rr_o\cos(\phi-\phi_o)+(z-\hat{z})^2}} \quad (48)$$

where $F(r_o,\phi_o)$, which has units of force/distance, can be expressed as a Fourier series

$$F(r_o,\phi_o)=\sum_{\nu=0}^{\infty}\cos\nu\phi_oF_\nu^c(r_o)+\sum_{\nu=1}^{\infty}\sin\nu\phi_oF_\nu^s(r_o) \quad (49)$$

For our purposes here

$$F_\nu^s(r_o) \equiv 0 \tag{50}$$

$$F_{\nu=0}^c(r_o) = \frac{(r_t - r_o)F^h + (r_o - r_h)F^t}{r_t - r_h} \tag{51}$$

which is a linear function with known values of sectional loads F^h, F^t, respectively, at $r_o = r_h$, r_t. Vector F_m for use in Eq. (24) is now replaced by F_m/F^t,

$$\frac{F_m}{F^t} = \frac{1^t}{\pi L}\int_0^\pi d\psi \sin\psi \sin[(m+1)\psi](\cos\psi - \hat{z}) \times \int_{r_h}^{r_t} dr_o \left\{\frac{(r_t - r_o)F^h/F^t + r_o - r_h}{r_t - r_h}\right) \times \int_0^\pi d\alpha e^{ikR}(a + r_o\cos\alpha)\left[-\frac{k^2}{R^3} - \frac{3ik}{R^4} + \frac{3}{R^5}\right] \tag{52}$$

where $R = [a^2 + r_o^2 + 2ar_o\cdot\cos\alpha + (\cos\psi - \hat{z})^2]^{1/2}$.

The total far field normalized by the on-axis incident field is given by

$$\lim_{R_o\to\infty} \frac{|p^{\text{inc}} + p^o|}{|p^{\text{inc}}(\theta = o)|} = \frac{1}{(r_t - r_h)} \frac{2}{(1 + F^h/F^t)} \times \left| i\cos\theta e^{-ik\hat{z}\cos\theta} \times \int_{r_h}^{r_t} dr_o \frac{(r_t - r_o)F^h/F^t + r_o - r_h}{r_t - r_h} J_o(kr_o\sin\theta) + \frac{\pi aL}{2}\sin\theta J_1(ka\sin\theta) \times \sum_{m=0}^{N} a_m(m+1)e^{\mp im\pi/2} \frac{J_{m+1}(|k\cos\theta|)}{|k\cos\theta|}\right| \tag{53}$$

where, as before, the $\mp$ signs on $\exp(\mp im\pi/2)$ correspond, respectively, to $\theta \lesseqgtr \pi/2$. In the above, a_m has dimensions of 1/distance, i.e., the units of ratio F_m/F^t in Eq. (52). Thus, in Eq. (53) the combination $L\cdot a_m$ is dimensionless.

Numerical Results for Single Driving Dipole

We now apply the theory to three different finite pipes of equal length insonified by a centerline dipole of strength F_o. The normalized "a" of the slenderest of the three is 2/13; the next in size is eight times greater, or 2/1.628, and the widest is greater yet by an additional factor of 2, with $a = 2/0.814$.

For the median case of $a = 2/1.628$, Table 1, demonstrating the validity of the calculation through the power balance discussed previously, shows a comparison of computed radiated and input powers as given by Eqs. (47) and (34). The axial source position is $\hat{z} = 1/2$. The second column contains the monotonically increasing reference power of the dipole in free field [Eq. (35)]. The associated diffraction loading Δp is plotted in Fig. 2 for the single normalized acoustic wavenumber $k = 8.3$, for which the ratio of cylinder to acoustic wavelength is about 2.5. The curves accordingly display a two-cycle variation and the local square root decay with distance to either end, as enforced by Eq. (20). Figure 3 shows directivity patterns for $k = 3.25$ and 8.3. Levels have been normalized by on-axis incident field values so that at $\theta = 0$, π both curves are zero in agreement with Eq. (17) and the discussion following it. Since the incident field vanishes at 90 deg, radiation levels there are due to contributions of only virtual sources, specifically to the spatial average of $\Delta p(z)$ over the cylindrical surface.

Table 1 Comparison of computed input and radiated powers

k	$\rho cL^2\Pi^{\text{inc}}/F_o^2$	$\rho cL^2\Pi_{\text{inp}}/F_o^2$	$\rho cL^2\Pi_{\text{rad}}/F_o^2$
3.24	0.556465E+00	0.230349E+00	0.230680E+00
3.32	0.585367E+00	0.820156E+00	0.822079E+00
3.41	0.615001E+00	0.113739E+01	0.113933E+01
3.49	0.645367E+00	0.102409E+01	0.102543E+01
3.57	0.676465E+00	0.976669E+00	0.977732E+00
3.65	0.708294E+00	0.971323E+00	0.972269E+00
3.74	0.740855E+00	0.957815E+00	0.958720E+00
3.82	0.774148E+00	0.899270E+00	0.900182E+00
3.90	0.808172E+00	0.804643E+00	0.805597E+00
3.99	0.842929E+00	0.716848E+00	0.717872E+00
4.07	0.878416E+00	0.667774E+00	0.668890E+00
4.15	0.914636E+00	0.668143E+00	0.669367E+00
.	.	.	.
.	.	.	.
8.3	0.365854E+01	0.345136E+01	0.345139E+01

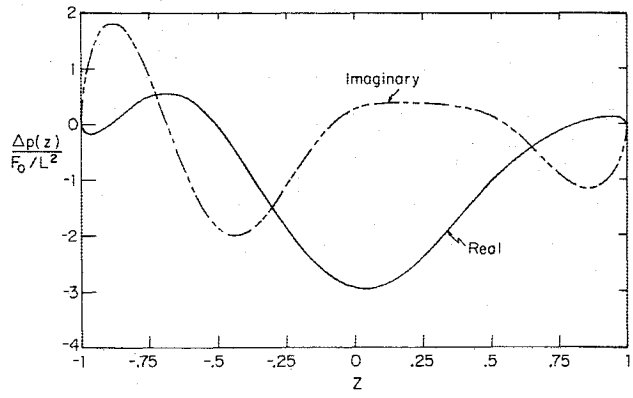

Fig. 2 Calculated virtual load $\Delta p(z)/(F_o/L^2)$ in linear scale (source of scattered field) for single-dipole incident field ($k = 8.3$, $\hat{z} = 1/2$).

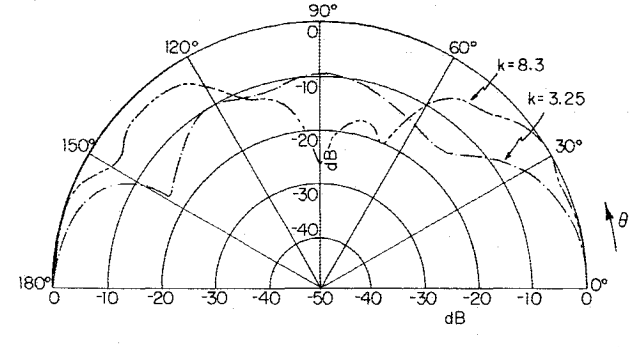

Fig. 3 Predicted directivity patterns (20 $\log_{10}|p(\theta)/p^{\text{inc}}(\theta = 0)|$) of total pressure for $k = 3.25$, 8.3 (using $\hat{z} = 1/2$).

Figure 4 shows computed power sweeps in logarithmic scale for the three cylinders in question with $\hat{z} = 1/2$. For each geometry the value of the first resonance corresponds to the plane-wave axial motion within the pipe. Levine and Schwinger's well-known conclusion that in the limit of small radius (low frequency) the reflection coefficient at the opening of a semi-infinite unflanged pipe, or horn, becomes -1 for such motion (Eqs. VI.2, VII.1 of Ref. 1) suggests that a condition close to pressure release should also exist at the two flat ends of the interior volume of the $a = 2/13$ geometry. Neglecting the effect of nonzero absorption at these two "end surfaces" (i.e., of their vanishing energy seepage to the exterior), one may take orthogonality to hold in an expansion of the interior pressure field in axial func-

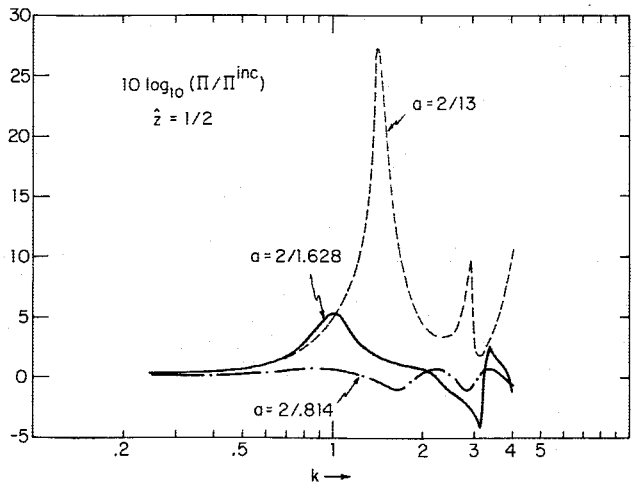

Fig. 4 $10\log_{10}(\Pi/\Pi^{inc})$, computed power normalized by insonifying dipole radiated power in free field for three different pipes ($\hat{z}=1/2$).

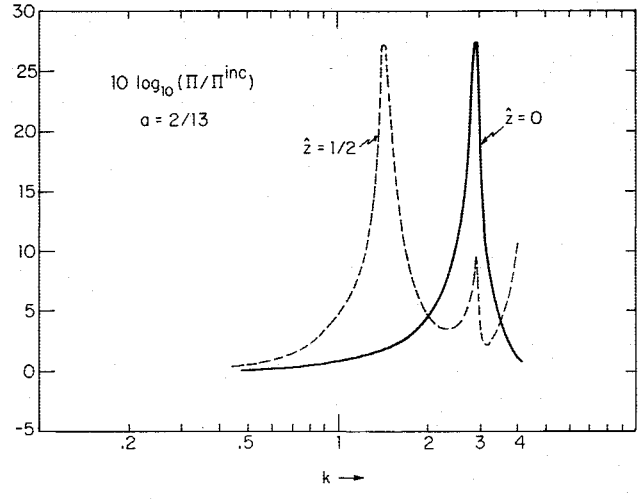

Fig. 5 Effect on radiated power of shifting source position from $\hat{z}=1/2$ to $\hat{z}=0$ for the $a=2/13$ pipe.

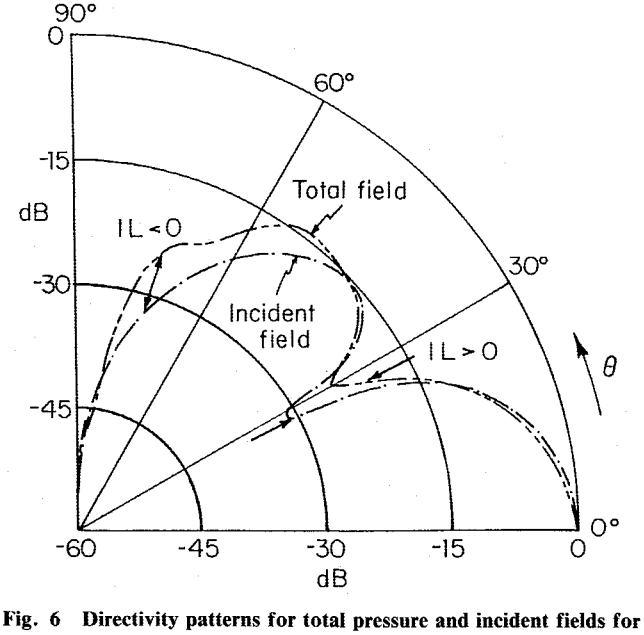

Fig. 6 Directivity patterns for total pressure and incident fields for a radial distribution of dipoles ($k=8.3$); Arrows indicate regions of negative and positive insertion loss.

tions $\sin(m\pi z_d/L)$, with "m" becoming formally real in the small-radius limit and z_d denoting axial dimensional distance measured from the cylinder's left end. For $\hat{z}\neq 0$ the first axial resonance occurs for $m\pi/L=k_d$ with $m=1$ and k_d equal to the dimensional acoustic wavenumber, $2k/L$. The corresponding result for k at the fundamental is $\pi/2$, a value almost reached by position of the first peak for the $a=2/13$ curve. The position of the first axial harmonic ($m=2$) appears at twice this number with a lower level. The generally higher peak powers for the slender cylinder are consistent with a system that is then almost perfectly reactive, with resonances and antiresonances predictably showing up as large excursions from the spectrum's mean line. The increased number of extrema apparent in the sweep of the widest pipe ($a=2/0.814$) is due to the higher modal density in the radial direction; the relatively shallow levels are caused by better impedance matching to the exterior space. Cut-on of the first radial mode is noted to occur at about $k=2.3$, as opposed to $k=3.5$ for the $a=2/1.628$ pipe of half the radius.

Figure 5 uses the $a=2/13$ slender geometry to show the effect of placing the driving centerline dipole at the cylinder midaxis $\hat{z}=0$. The incident field is then axially antisymmetric about $\hat{z}=0$ and in the low-frequency or small-radius limits excites only even-m values of the $\sin(m\pi z_d/L)$ functions. The first axial resonance corresponds to $m=2$ and for $a\ll 1$ should occur at $k=\pi$. The curve shows a shift down from this limiting value to about 2.9; the level, however, appears roughly unchanged from that at $k=1.4$ for the $\hat{z}=1/2$ case.

Numerical Results for Radial Distribution of Blade Thrusts

As a brief application of the blade-thrust model we now analyze the $a=2/1.628$ geometry with $r_h/a=0.2125$, $r_t/a=0.685$ $[r_t=r_h+(a-r_h)\times 60\%]$. We assume that sectional loads F^t, F^h are in phase so that F^h/F^t is real and has the value of 0.2. The axial position of blade sources is now taken to be $\hat{z}=0$. Because the virtual loading on the cylindrical surface is antisymmetric with respect to the $z=0$ plane, both incident and diffracted fields vanish for $\theta=90$ deg and are symmetric relative to $\theta=90$ deg. Figure 6 shows the total and incident fields normalized by the on-axis value of the latter for $k=8.3$. The gap between the curves is a spatial plot of acoustic insertion loss provided by the diffracting surface. The regions of positive and negative values are indicated by arrows.

Conclusions

The diffracted field for a rigid, open-ended pipe of zero thickness and finite length has been calculated for a moderate range of frequencies, and shown to vanish along the axis of the cylinder, which provides zero insertion loss at these points.

The problem was posed and solved as a lifting surface that must cancel an imposed incident downwash field. The calculated virtual load, or source of the scattered pressure component, was checked by verifying that its effect on the near-field input power at the actual source (a force dipole) is consistent with the far-field power radiated by the system. Such a balance is possible only if the boundary behaves reactively always (an unlikely coincidence for all frequencies computed), or if the no-flow-through boundary condition has been satisfied correctly over the rigid pipe surface so that the velocity part of the acoustic intensity is identically zero.

We also applied the model to isolate the purely diffracting effect of an idealized cylindrical shroud, or duct, on the axisymmetric component of unsteady blade thrusts for a fan. The insertion loss was observed to be a complicated function of space and frequency, able to yield both positive and negative values depending on far-field angular position.

References

[1]Levine, H. and Schwinger, J., "On the Radiation of Sound from an Unflanged Circular Pipe," *Physical Review*, Vol. 73, No. 4, Feb. 1984, pp. 383–406.

[2]Bouwkamp, C. J., "Diffraction Theory," *Reports on Progress in Physics*, Vol. 17, 1954, pp. 35–100; (cf. discussion just before his Eq. 2.11.)

[3]Watkins, C. E., Runyan, H. L., and Woolston, D. S., "On the Kernel Function of the Integral Equation Relating the Lift and Downwash Distribution of Oscillating Finite Wings in Subsonic Flow," NACA Rept. 1234, 1955.

[4]Schuster, G. T. and Smith, L. C., "A Comparison Among Four Direct Integral Equation Methods," *Journal of the Acoustical Society of America*, Vol. 77, March 1985, pp. 850–864.

[5]Schenck, H. A., "Improved Integral Formulation for Acoustic Radiation Problems," *Journal of the Acoustical Society of America*, Vol. 44, Feb. 1968, pp. 41–58.

[6]Burton, A. J. and Miller, G. F., "The Application of Integral Equation Methods to the Numerical Solution of Some Exterior Boundary-Value Problems," *Proceedings of the Royal Society of London*, A323, 1971, pp. 201–210.

[7]Mathews, I. and Hitchings, D., "Acoustic Radiation for Three-Dimensional Elastic Structures," *Innovative Numerical Analysis for the Engineering Sciences*, Univ. of Virginia Press, 1980, pp. 69–78.

[8]Reut, Z., "On the Boundary Integral Methods for the Exterior Acoustics Problems," *Journal of Sound and Vibration*, Vol. 103, No. 2, Nov. 1985, pp. 297–298.

[9]Hamdi, M. A. and Ville, J. M., "Sound Radiation from Ducts: Theory and Experiment," *Journal of Sound and Vibration*, Vol. 107, June 1986, pp. 231–242.

[10]Horowitz, S. J., Sigman, R. K., and Zinn, B. T., "An Iterative Finite Element-Integral Technique for Predicting Sound Radiation from Turbofan Inlets in Steady Flight," *AIAA Journal*, Vol. 24, Aug. 1986, pp. 1256–1262.

[11]Nayfeh, A. H., Kaiser, J. E., and Telionis, D. P., "Acoustics of Aircraft Engine-Duct Systems," *AIAA Journal*, Vol. 13, Feb. 1975, pp. 130–153.

[12]Fuller, C. R., "Propagation and Radiation of Sound from Flanged Circular Ducts with Circumferentially Varying Wall Admittances, II: Finite Ducts with Sources," *Journal of Sound and Vibration*, Vol. 93, April 1984, pp. 341–351.

[13]Prasad, M. G., "A Four Load Method for Evaluation of Acoustical Source Impedance in a Duct," *Journal of Sound and Vibration*, Vol. 114, April 1987, pp. 347–356.

[14]Orszag, S. A. and Crow, S. C. "Instability of a Vortex Sheet Leaving a Semi-Infinite Plate," *Studies of Applied Mathematics*, Vol. 49, 1970, pp. 167–181.

[15]Crighton, D. G., "Radiation Properties of the Semi-Infinite Vortex Sheet," *Proceedings of the Royal Society of London*, A330, 1972, p. 185.

[16]Crighton, D. G., "The Excess Noise Field of Subsonic Jets," *Journal of Fluid Mechanics*, Vol. 56, pp. 683–694.

[17]Munt, R. M., "The Interaction of Sound with a Subsonic Jet Issuing from a Semi-Infinite Cylindrical Pipe," *Journal of Fluid Mechanics*, Vol. 83, 1977, pp. 609–640.

[18]Abramowitz, M. and Stegun, I., *Handbook of Mathematical Functions*, Dover, 1968.

[19]Martinez, R., "Formulation for the Diffracted Field of an Open-Ended Pipe," CAA Rept. U-1357-351, April 1986.

[20]Noble, B., *Methods Based on the Wiener-Hopf Technique*, Pergamon, 1958, pp. 31, 34 (Eqs. 1.56, 1.71).

[21]Pierce, A. D., *Acoustics, An Introduction to Its Physical Principles and Applications*, McGraw-Hill, New York, 1981, p. 167 (Eq. 4-4.5).

[22]Lamb, H., *The Dynamical Theory of Sound*, Dover, 1960, p. 239 (Eq. 3).